

A Theoretical Study of the Influence of the Injection Velocity on the Heat and Fluid Flow in A Soaking-Pit Furnace when using Flameless Oxyfuel Heating

Par Jonsson¹, Patrik Ound² and Nils.A.I Andresson³

¹ KTH Royal Institute of Technology

Received: 11 December 2016 Accepted: 2 January 2017 Published: 15 January 2017

Abstract

Flameless oxyfuel combustion is one of the most recently developed combustion systems that has the potential to provide better combustion efficiency combined with a lower pollution production compared to conventional combustion systems. However, a lack of knowledge exists with respect to the influence of different parameters on the combustion results when using the flameless oxyfuel technology. Thus, in the current study a previously validated CFD model is used to investigate the effect of the injection velocity on the temperature distribution, recirculation ratio of the flue gases, flame volume, turbulence intensity, and flame radiation to the ingots. The results show that an increased injection velocity highly affects the temperature uniformity inside the chamber. More specifically, the maximum temperature difference in the flame region drops from 8.59

Index terms— soaking PIT furnace, CFD, oxy-fuel combustion, flame, heat transfer.

1 I. Introduction

In the process of producing steel and billets from scrap iron, the soaking pit furnaces are used to preheat the cast ingots after the casting process to provide for optimum temperature conditions before the rolling process. The latter process provides the desired metallurgical properties in the final products, so the input conditions for the rolling process are important. Therefore, the operational condition of the soaking process such as the efficiency of the combustion, uniformity of temperature and heat transfer, flame shape and flue gas composition largely influences the total energy consumption and pollution generation.

One promising method to control the pollution and to increase the combustion efficiency is to replace the air by a pure oxygen gas as the oxidant. This method was investigated intensely by International Flame Research Foundation (IFRF), where they focused on different aspects such as the measuring equipment, combustion characterization, CFD development and validation (1).

Examples of studies on the subject include the study of Buhre et al. (2) in 2015 and the study by Kim, Kim et al (3) in 2007. More specifically, Buhre et al. (2) studied the effect of employing the oxyfuel systems as a method for CO₂ sequestration (2). Furthermore, Kim, Kim et al (3) investigated the effect of oxyfuel combustion with external flue gas recirculation systems on the NO emission, based on an experimental work. They also investigated the oxyfuel burner flame stability for different external recirculation rates (3).

Wall et al. (4) also studied the effect of the gas recirculation inside the flame region on combustion. They concluded that the gas recirculation controls the flame temperature and flow pattern of the flue gases (4). In another experimental study, Andresson et al. (5) compared the combustion chemistry in conventional airfuel combustion with the oxyfuel burner combustion. They concluded that the oxyfuel combustion system produces up to 30% less NO_x emissions in comparison to the identical air combustion system (5). Kim 2010, Toftegaard et al. (6) carried out a comprehensive literature study on the subject of oxyfuel combustion and claimed that a big

43 lack of research existed in the area (6). Beside this study, many numerical investigations were also published to
44 study oxyfuel combustion (7) (8) (9). Also, many studies were focused on validating suitable CFD models to use
45 for simulating the complicated case of oxyfuel combustion. In 2010, Johansson et al. (10) studied the effect of
46 different radiation models on combustion when using oxyfuel burners and they compared predicted and measured
47 data. More specifically, they studied special radiative characterization of flue gases in oxyfuel combustion and
48 concluded that the Weighted Sum of the Gray Gases Model (WSGGM) is the most relevant radiation model to
49 use (11). In 2012, Hjartstam et al. (12) also carried out work to validate radiation models used to simulate
50 oxyfuel combustion. They concluded that the graygas model is not sufficiently accurate to be used for this
51 purposes compared to the non-gray gases model (13). In 2013, an investigation on a suitable combustion model
52 was also enrolled by Alletti et al. (14). They reported that if it is necessary to consider a fast chemistry this
53 will significantly reduce the accuracy in predicting the temperature when using oxyfuel combustion (15).

54 In general, many advantages are associated with using oxyfuel combustion compared to aircombustion.
55 These include a higher productivity, a higher flame temperature and thermal efficiency, a better radiative
56 characterization of the flue gases, lower exhaust gases volume, and improved flame stability (16).

57 As the industry has started to use this combustion system, some practical issues have also observed. Mainly
58 the issues were concerning the high NOx production, in case of air leakage into the combustion chamber. This
59 emphasized that the lack of convective effects and high local temperature leads to the production of thermal
60 NOx in industrial applications. This issue is extensively described in the work by Redriksson et al. (17). They
61 studied the effect of air leakage on the total NOx formation and reported that the sharp temperature gradient
62 in the flame area produces a large amount of NOx during the combustion. Buhre et al.

63 (18) also investigated some issues associated with the use of oxyfuel combustion with respect to the heat transfer,
64 flame stability and gaseous emissions (19). Since the formation rate of thermal NOx is an exponential function of
65 the flame temperature and a square root function of the oxygen concentration, it can be extremely reduced by
66 controlling the flame temperature or by diluting it (20).

67 Based on the above described drawbacks with the oxyfuel combustion technology, a modified burner design was
68 introduced by IFRF, namely the flameless oxyfuel technology (21). In this combustion system, a high Internal
69 Flue Gas Recirculation (IFGR) is forced to the system to produce a leaner combusting mixture. The idea is
70 to produce a low concentration of reactant so that the combustion is not initiated before the mixing process
71 is completed (22). After reaching the autoignition temperature within the mixture, reactions takes place in a
72 diluted manner. The flame in such combustion systems is very spread as well as it is invisible to the naked eye.
73 This type of combustion, which can be implemented in both air oxidation combustion and oxyfuel combustion,
74 is called flameless combustion (23).

75 The special aspects in these type of furnaces are two folded; an asymmetric and especial design of the injection
76 nozzles, and very high (near-sonic) injection velocity of fuel and the oxidant. These aspects lead to the formation of
77 a volumetric flame configuration that -in case of correct adjustments-results in a uniform temperature distribution
78 and a lower local temperature within the flame. In this manner the high radiative bulk of flue gases turn into a
79 volumetric flame which is the source of radiation inside the chamber (24).

80 Even though the flameless combustion technology is very young, it is already widely used in many industrial
81 applications. Examples of applications in the steel industry are: walking beam and catenary furnaces at
82 Outokumpu in Avesta, soaking pit furnaces at Ascometal, Rotary heart furnaces at ArcelorMetal in Shelby,
83 and soaking pit furnaces at Ovako Sweden (25), Hofors (26).

84 This implies the necessity of filling the gaps of knowledge about this modern combustion technology, since
85 there are very few studies done on the subject. In 2006, Vesterberg et al. (27) studied 10 full scale reheating
86 and annealing furnaces equipped with flameless oxyfuel burners. They concluded that the use of this technology
87 had many advantages such as: a more uniform heat transfer, a shorter heating time and consequently lower
88 energy consumption, an ultra-low NOx formation. In addition, Krishnamurthy et al. (28) compared different
89 combustion systems including flameless oxyfuel and High Temperature Air Combustion (HiTAC) burners with
90 respect to their thermal efficiency, in-flame temperature distribution, heat flux, gas composition and NOx
91 emissions (29). They used a semi-industrial furnace equipped with flameless oxyfuel burners. These results
92 were later used by Hadamgahi et al. (30) to validate a CFD model for modeling flameless oxyfuel combustion
93 in a soaking pit furnace equipped with flameless oxyfuel burner in Ovako Sweden AB.

94 In this study, the previously validated CFD model (31) is used to investigate the effect of the burner capacity
95 on the temperature distribution profile, radiation profile and the overall operational conditions of the combustion
96 system.

2 II.

3 Mathematical Modeling

99 A 3-dimensional mathematical model was developed to simulate the combustion and turbulence by using Ansys
100 Fluent 16.0. The equations were solved by considering the system to be in a steady state. It was also assumed
101 that the flue gas mixture behaved like a perfect gas mixture. The following governing equations were solved:

102 Based on these assumptions, the following governing equations were solved: Continuity equation: $\nabla \cdot (\rho \mathbf{u}) = 0$
103 (1)

104 Momentum equation: $\rho \left(\frac{d\mathbf{u}}{dt} + \mathbf{u} \cdot \nabla \mathbf{u} \right) = -\nabla p + \nabla \cdot \boldsymbol{\tau} + \rho \mathbf{g}$ (2)

105 Energy balance equation: $\rho c_p \left(\frac{dT}{dt} + \mathbf{u} \cdot \nabla T \right) = \nabla \cdot (\mathbf{k} \cdot \nabla T) + \dot{q}$ (3)

106 where \mathbf{u} is the velocity vector (m/s), ρ is the density (kg/m³) and $\boldsymbol{\tau}$ is the stress tensor. Furthermore, $\rho \mathbf{g}$

107 and p are the gravitational body forces and the pressure (Pa), respectively. In addition, \mathbf{k} represents the thermal

108 conductivity (W/m²K), and c_p defines the heat capacity at a constant pressure (J/kg²K) [26]. Also \dot{q} counts

109 for any volumetric heat sources. Regarding the incompressible behaviour of the flow, the Navier Stokes equation

110 is solved, which can be written as follows: $\nabla \cdot \boldsymbol{\tau} = \rho \mathbf{g} + \rho \mathbf{g}$ (4)

111 where the parameter \mathbf{g} represents the gravity and ρ is thermodynamic work on the system. Furthermore, the

112 parameter $\nu = \mu / \rho$ is the kinematic viscosity (18).

113 The flow was assumed to be fully turbulent, incompressible and the diffusion coefficients for all the gaseous

114 products were assumed to be equal. Therefore, turbulence was modeled by using a Realizable $k-\epsilon$ turbulence

115 model to solve the Navier-Stokes equations. This selection of the sub-model is extensively explained in the work

116 by Hadamgahi et al. (19). However, it can briefly be stated that in this model the kinetic energy (k) and the

117 turbulent dissipation rate (ϵ) were solved as shown in equation 5 and equation 6: $\frac{dk}{dt} + \mathbf{u} \cdot \nabla k = P_k - \epsilon + \nabla \cdot (\mathbf{k}_t \cdot \nabla k)$

118 $\frac{d\epsilon}{dt} + \mathbf{u} \cdot \nabla \epsilon = C_{\epsilon 1} \frac{\epsilon}{k} P_k - C_{\epsilon 2} \frac{\epsilon^2}{k} + \nabla \cdot (\mathbf{k}_t \cdot \nabla \epsilon)$ (5) $\frac{d\epsilon}{dt} + \mathbf{u} \cdot \nabla \epsilon = C_{\epsilon 1} \frac{\epsilon}{k} P_k - C_{\epsilon 2} \frac{\epsilon^2}{k} + \nabla \cdot (\mathbf{k}_t \cdot \nabla \epsilon)$

119 $\frac{d\epsilon}{dt} + \mathbf{u} \cdot \nabla \epsilon = C_{\epsilon 1} \frac{\epsilon}{k} P_k - C_{\epsilon 2} \frac{\epsilon^2}{k} + \nabla \cdot (\mathbf{k}_t \cdot \nabla \epsilon)$ (6)

120 Where $C_{\epsilon 1} = \max(0.43, 1.5)$, $C_{\epsilon 2} = 1.0$, $C_{\epsilon 3} = 1.2$, $C_{\epsilon 4} = 1.9$, $C_{\epsilon 5} = 1.44$

121 and \mathbf{k}_t is described by equation (6): $\mathbf{k}_t = \frac{\nu^2}{k} \left(\frac{P_k}{\nu} - \epsilon \right) \mathbf{I}$ (6)

122 The combustion was solved by using a SLFM to solve the PDF. The developed model also treats the combustion

123 chemistry, departed from the chemical equilibrium, which is a necessary consideration in modeling flameless

124 combustion systems [19]. In this mathematical solution, the thermochemistry parameters are a function of both

125 the mixture fraction and the dissipation rate (ϵ), which are described in equations 7 and 8, respectively: $\delta = \frac{\epsilon}{k}$

126 $\delta = \frac{\epsilon}{k}$ (7) $\delta = \frac{\epsilon}{k}$ (8)

127 where δ is the diffusion coefficient.

128 It is important to note that in this study the infiltration of air was assumed to be negligible and NO_x products

129 were not considered.

130 The radiative Transfer Equation (RTE) was solved, using the DO model. In oxyfuel combustion systems the

131 flue gas radiative properties are strongly promoted compared to conventional air-fuel combustions. It is also

132 unsatisfactory for the predictions to consider the non-gray gas model (8). In this regards the WSGGM was also

133 considered to count for the variation of the absorption coefficient of the flue gases. The accuracy of using his

134 model in oxyfuel combustions has been investigated in many former studies (20) (21) (22) (23) (19). Also, the

135 total emissivity over the distance s can be presented as follows (4): $\epsilon = \sum_i \epsilon_i \left(1 - \exp(-\kappa_i s) \right)$

136 (9)

137 where ϵ_i stands for the emissivity weighting factor for the i th fictitious gray gas and the quantity in the

138 bracket stands for the i th fictitious gray gas emissivity. Furthermore, κ_i is the absorption coefficient of the i

139 th gray gas, p is the summation of the partial pressure of all absorbing gases, and s is the path length (19).

141 4 III.

142 5 Materials and Methods

143 6 a) Soaking pit furnace

144 The experimental work that has been done on a soaking pit furnace in Ovako Sweden AB, is extensively described

145 in refernces (28) and (25). These furnaces are used to provide preheating on the ingots in order to prepare

146 them for the rolling process. The furnaces are made of four cells which have a rectangular shape with a total

147 volume of 14.11 m³. Figure 1 shows the configuration of one cell including the ingots. Each cell accomodates 6

148 ingots that seat inside the chamber with the aid of automatic hooks. During the heating, the soaking time and

149 soaking temperature are essential parameters, that are set corresponding to the special type of the steel grade

150 and the desired final steel properties (18).

151 The soaking pit furnaces in Ovako Sweden AB, are all equipped with REBOX® flameless oxyfuel burners that

152 uses pure oxygen as the oxidant and LPG No.95 as the fuel (18). The injection velocity of the fuel and oxygen

153 may easily be adjusted by the operators. The maximum burner capacity is 900 kW. However, in the soaking pit

154 furnaces in Ovako, a lower amount (560 kW) is used to accomplish a flameless oxyfuel combustion. This burner is

155 mounted on the frontal wall of the chamber, where both the controlling thermocouple and the exhaust channel

156 are located. The controlling thermocouple is located 400 mm below the center of the burner and it continuously

157 monitors the temperature (18).

158 The quality of operational conditions of the furnace has a major effect on the soaking cost and quality.

159 Specifically factors such as the temperature and heat transfer uniformity inside the chamber, the level of

160 pollution production, and combustion efficiency determines the overall state of the furnace effectiveness. The

161 refractory walls are made of 230 mm AK60 A, 115 mm Porosil and Skamolex 1100 in 450 and 200 mm at the

162 transverse and longitudinal walls, respectively. The experimental work which has been done in Ovako Sweden

163 AB, is explained in detail in the work by Hadamgahi et al. (18). For the experimental result used in the current

164 study the local temperature of the flue gases was measured by using shielded S-type thermocouples. In addition,
 165 the locations of the sampling was carefully selected to provide a comprehensive view of the temperature profile
 166 inside the chamber. Overall, eight thermocouples were inserted to the furnace from the top side. These were
 167 divided in two different groups that were located at two different levels inside the chamber. These levels are called
 168 the High and Low levels, which are located at the heights of 2016 mm and 1065 mm, respectively. The exact
 169 position of the probes are given in Table 2 and c) Geometry and mesh ICEM 13 was used to draw the geometry
 170 of the furnace as well as the mesh structure. Note, that the configuration of the ingots inside the chamber is
 171 simplified in this scheme compared to the original arrangement. More specifically, the ingots were assumed to
 172 be standing up in the chamber and therefore the effect of leaning them towards the walls was neglected. This
 173 helps to decrease the number of nodes from 980000 to 850000, which consequently reduces the computational
 174 costs (25).

175 A study on the grid independancy of the mesh was also done (18) by observing the results of the simulation
 176 from two mesh configurations, namely tetragonal mesh and hexagonal mesh.

177 The unstructured tetrahedron mesh with a combination of the O-rings (Figure 3) for the inlet area was reported
 178 to be the best choice, regarding both the time required for a converged solution and an acceptable prediction
 179 accuracy (25). Also, the minimum orthogonal quality was 0.84, which is adequate according to the previously
 180 presented results (18) (19). The boundary conditions for the reference case at the inlets are shown in Table
 181 1. These data are taken from the operational conditions of the furnace at the plant. They were used in the
 182 simulations made by ??hadamgahi et al. (18) in order to validate sub-models for simulating the flameless oxyfuel
 183 burner at Ovako Sweden AB. In order to study the role of the burner capacity on the combustion, six cases with
 184 different inlet boundary conditions were simulated. The burner capacity in these cases gradually increased from
 185 130 kW in case 1 to 907 kW in case 6. Also, the mass rate for fuel and oxygen was calculated according to the
 186 corresponding burner capacity by assuming a constant lambda value for all the cases. These data are shown in
 187 Table 2. It is important to note that the mentioned inlet boundary conditions are used to demonstrate that the
 188 flameless oxyfuel mode, which is applied after the chamber, reaches the self-ignition temperature. The ingots are
 189 also considered as heat sinks, with a separate constant heat flux for each ingot. The procedure of calculating
 190 these magnitudes is extensively explained in the work by ??hadamgahi et al. (18). In this assuming a fixed
 191 temperature for each of the ingots during the entire heating period. The final magnitudes for all the ingots are
 192 shown in Table ?? (18). The ingots' marking is illustrated in Figure 4. In the simulation, fuel and oxygen are
 193 not preheated and therefore they enter the chamber at 22°C and 25°C, respectively. Also, the refractories are
 194 defined as heat sinks with constant heat fluxes. These magnitudes are computed regarding the material of the .

195 Table ??: Maximum deviation between the CFD predictions and experimental data (18)

196 As shown in the table 5, the deviations between the predicted and measured temperatures varied between 3.47%
 197 and 9.95 %, which is considered to be fairly small for this type of furnace. Thus, the authors feel comfortable
 198 that the model can be used to make reliable predictions of temperatures in soaking pit furnaces.

199 7 b) Temperature Distribution And IFGR

200 An increase of the burner capacity when using flameless oxyfuel burner combustion highly affects the temperature
 201 distribution, flame shape and the flame temperature. Figure 5 shows the results for predicted temperature at
 202 the centerline of the furnace for all the studied cases. The line of representation starts from the burner face on
 203 the frontal side and ends at a position of 2000 mm from the back-wall. A very rapid increment for temperature
 204 is seen in regions very close to the burner side, which stands for the formation of the reaction zone for all the
 205 cases. This is followed by a rapid decrement for the temperature values at a distance of 500mm from the burner.

206 8 G

207 This figure indicates that the temperature uniformity is improved by increasing the inlet velocities of oxygen and
 208 fuel, as the temperature difference on the centerline decreases from 13% for case 2 to 8 % for case 6. This velocity
 209 increase leads to formation of a leaner reacting mixture and lower concentration of O₂ with a colder but more
 210 uniform flame. These results also show the effect of higher velocity on reducing the flame temperature in cases
 211 5 and 6, which is in good agreement with the work done by ??ilani et al (26). Also in 2016, ??hadamgahi et
 212 al. (25) reported results on the influence of the lambda value on the operational conditions in form of increasing
 213 the inlet oxygen mass rate. More specifically, they looked into the effect of increasing inlet velocities on the
 214 temperature distribution and consequently the exhaust losses. They also reported that although an increased
 215 oxygen velocity leads to a larger exhaust loss by 9.2%, it improves the temperature uniformity by 28%.

216 In order to further study the relevance between a total increase of the burner capacity and flame character-
 217 ization, Figure 7 Shows the temperature distribution profile for the selected cases of 1, 2, 5 and 6 at a middle
 218 plane on a z-y axis.

219 The maximum temperature in the flame region is highly dependent on the injection velocity. More specifically,
 220 this temperature is increasing while moving from case 1 with 130 kW to case 4 with 518 kW (1785 °C to 1820 °C).
 221 Afterwards, this temperature is decreasing from case 4 with 518 kW (1820 °C) to case 5 with 717 kW (1812 °C)
 222 and case 6 with 907 kW (1799 °C). Also, the maximum difference (between the peak and chamber temperature)
 223 for cases 1, 2 and 3 are 255°C, 242 °C and 235°C, respectively. This magnitude for cases 5 and 6 is seen to be

172 °C and 149 °C, which is considerably smaller compared to the other cases. Figure 6 shows the magnitudes of these values with respect to the percentage of the temperature deviation at the centerline. As it is shown in Figure 7, an increase of the injection velocities leads to the formation of a more turbulent mixing flow and a better recirculation of gases inside the chamber. In Case 3, especially in areas with fluid impinging effect, a wider range of temperature spectrum (temperature difference of 422°C) on this z-y plane is seen. Although a less temperature difference exists in case 6 (384°C), due to formation of large eddies and turbulence intensity. Figure 8 shows the predicted values of the turbulence intensity (%) for all the cases, in the length of the chamber. As shown in Figure 8, turbulence intensity dramatically increases with an increased injection velocity, in the flame region (50-400 mm away from the burner). This effect, which is in line with the predicted results for temperature, shows the effect of turbulence in making a more uniform temperature distribution. Additionally, Figure 9 shows the temperature profile on an x-z plane in the middle of the furnace. A higher degree of volumetric flame is expected to form by going from case 1 to 6 (increasing injection velocities), according to the results in this figure. However, the flame impinging effect on the rear wall suppresses this effect due to the chamber configuration. In the previous studies brought in sections 5 and 6 (supplements 2 and 3) the effect of a flame impingement on the temperature distribution was argued. Although this effect is neglected in this study, as Figure 8 reports the turbulence far away from the impinging side. In a flameless oxyfuel combustion, the chemical reactions happens with departure from chemical equilibrium, since the gas mixture of the reactants is leaned with recirculated flue gases. This is due to that the IFGR inside the chamber in the neighborhood of the flame region is increased (26). In this regard one of the most important factors for determining the flameless behavior of the combustion is the value of the recycle ratio of the combusting gases. This value was introduced by Hasegawa et al. (1997) as: $k_v = \frac{M_e}{M_a + M_f}$ (10) where M_e is the internal exhaust gases flow rate that is recirculated into the mixing reactants before a reaction takes place. Furthermore, M_a is the combustion oxygen flow rate, and M_f is the fuel flow rate. Combustion is conventionally stable for $k_v < 0.3$, although for $k_v > 0.3$ temperature of the furnace determines the stability of the flame (3). Higher recirculation of the flue gases threatens the flame stability and can even result in a flame lift-up and a blow-out case of a chamber temperature lower than the self-ignition temperature (29). Therefore, using a stable combustion with a high IFGR value is only beneficial in case of a sufficiently high temperature in the chamber (reactants temperature > 700 °C). This, on the other hand, stresses the necessity of defining a gradual combustion process in order to avoid to operate the burner in the flameless mode in a cold chamber.

9 c) Flame shape and total radiation on the ingots

Heat transfer inside the industrial furnaces is mainly carried out by two heat transfer methods, namely radiation and convection. Naturally the most effective parameters that influence the heat transfer ratio are the: i) flame temperature, ii) flame shape and emissivity, iii) ingots' initial temperature and emissivity, and iv) the temperature and emissivity of the walls. Oxygen content in the oxidizer plays an essential role in the final radiative fluxes from the flue gases, since it attains the final radiative properties of the flue gases. More specifically, by using oxygen as the oxidant instead of air a significant increment in the total flue gas emissivity is obtained. It also causes a significant decrement in the total flue gas volume, compare to air-fuel combustion systems. Another special aspect of using flameless oxyfuel flames is the formation of a widespread flame shape with a lower peak temperature, as shown in Figure 8. This figure is taken from the work by Lasia et al. (31). This ideally turns the flame into a large radiation source that has a uniform temperature, which highly influences the uniformity of the heat transfer. Overall, in flameless oxyfuel combustion flame has a lower temperature, but a more volumetric shape. These factors change the behavior of heat exchange between the flame and the ingots inside the chamber. Since the flame is the main radiation source, the heat is transferred to the slabs directly from the flame and indirectly from the walls. Thereby a net heat flux from the flame to ingots can be obtained from the following correlation (31): $q_{net} = q_{F \rightarrow I} - q_{I \rightarrow F} = A_F \epsilon_F (T_F^4 - T_I^4) - A_I \epsilon_I (T_I^4 - T_W^4) = A_F \epsilon_F T_F^4 - A_I \epsilon_I T_I^4 + A_I \epsilon_I T_W^4 - A_I \epsilon_I T_I^4$ (19)

The subscripts F, I and W correspond to the flame, ingots and refractory wall respectively. Furthermore, T_W is the furnace wall temperature (K), T_F is the flame temperature (K), and T_I is the ingots' temperature (K). Finally, ϵ_W , ϵ_I and ϵ_F are the emissivity values of the walls, ingots and flame respectively. The parameter C is the Stefan-Boltzmann constant. With the assumption of $\epsilon_F = 0.25$, $\epsilon_W = 0.8$ and $\epsilon_I = 0.85$, respectively, and assuming the flame having a cylindrical shape, the total heat transferred from the flame to the ingots (kW) can be described as follows (31): $Q_{net} = A_F \epsilon_F T_F^4 - A_I \epsilon_I T_I^4 + A_I \epsilon_I T_W^4 - A_I \epsilon_I T_I^4 = C 4V_F D$ (19)

understood that having a flame impinging effect on a refractory wall and formation of a thick thermal boundary layer, makes that area a compacted radiative source that jeopardizes the radiation uniformity (32).

In order to investigate this effect, we consider the entire flame as a volumetric source of radiation to the surroundings. Thus, the radiated energy from the flame can be expressed as follows: $Q_{rad} = Q_{F \rightarrow F} + Q_{F \rightarrow I} + Q_{F \rightarrow W} = Q_{F \rightarrow F} + Q_{F \rightarrow I} + Q_{F \rightarrow W}$ (20) $D = Q_{rad} / Q_{F \rightarrow F} = T_F^4 / T_I^4$ (21)

This can lead us to the following function for the flame volume: $V_F = D Q_{F \rightarrow F} / C 4V_F D$ (22)

Figure 15 shows the relevance between the flame volume, Q_{rad} and D , for all the studied cases.

10 G

284
285
286
287
288
289
290
291
292
293
294
295
296
297
298
299
300
301
302
303

where ϵ is the Planck mean absorption coefficient for an optically thin flame. This simplification leads us to the introduction of a known term "D", based on the study done by Burns in 1996 (32). D is defined as the ratio of the radiant heat transfer rate from the flame to the surroundings (Q_{rad}) to the total heat released by the flame (Q_0), and it can be written as follows:

where V_F , d_F and l_F stand for the flame volume, flame diameter and flame length, respectively. This equation illustrates the importance of the role of the wall temperature and flame temperature on the incident radiation on the ingots' surfaces. As if the combustion happens in a flameless manner, with a low and wellspread volume, the radiation is more uniform on the ingots. On the other hand, a high peak temperature in the flame area has an opposite effect. It can also be

This figure demonstrates the effect of flame volume on total radiation, meaning an increased flame volume increases the total radiation from the flame. It is also seen that the increase in the ratio between the radiative heat transfer and total released heat from the flame loses its significance after a radiation value of 700 kW. This calculation is done by assuming a 100% combustion efficiency.

In a general view, with the increase of flame volume, temperature drops, but total radiation heat flux increases (31). Burns 2007, Blasiak et al. (31) carried out the same calculations with the focus on studying the effect of gas emissivity and flame volume on the total heat transfer. They concluded that when the gas temperature distribution inside the furnace chamber (well stirred reactor) is uniform, the effect of the flame emissivity becomes smaller than the effect of the flame volume (31).

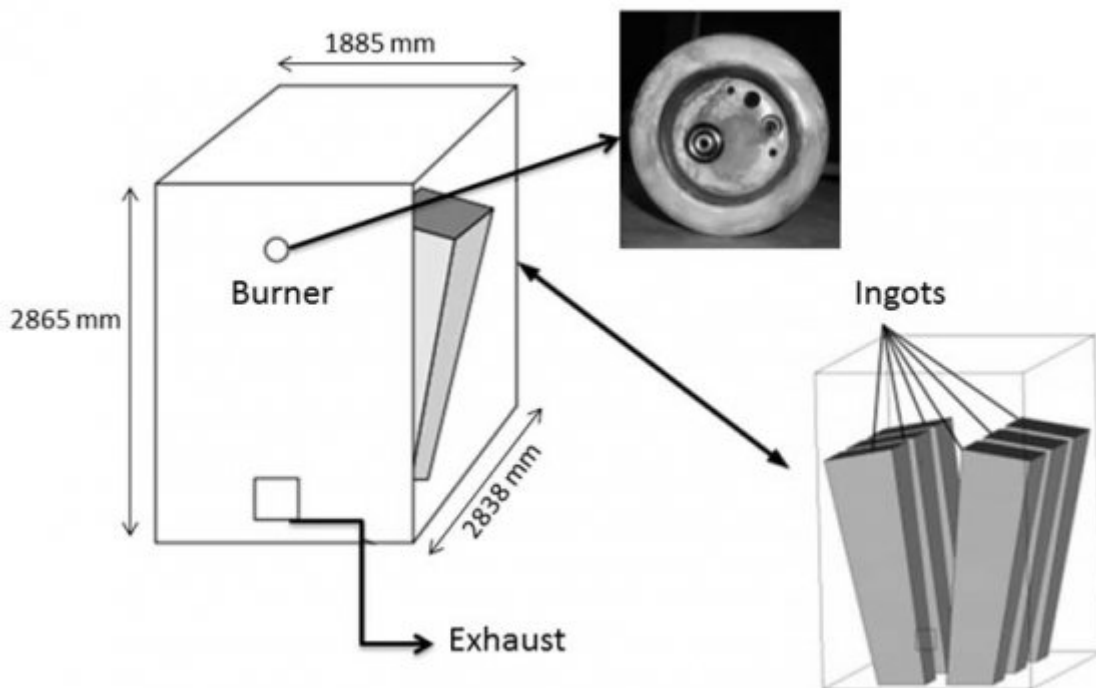
V.

11 Conclusions

304
305
306
307
308
309
310
311
312
313
314
315

The aim in the current study was to simulate flameless oxyfuel combustion using a previously validated CFD model. More specifically, the focus was to investigate the effect of the injection velocity on the temperature distribution, flame temperature, flame volume, turbulence intensity, and flame radiation to the ingots. Based on the results of this study, the following main conclusions may be drawn:

An increase of the injection velocity highly affects the flame temperature and temperature uniformity inside the chamber as the maximum temperature difference in the flame region drops from 14% to 8% for burner capacities of 130 kW and 907 kW, respectively. The formation of a more uniform temperature profile when using a higher burner capacity of 907 kW instead of a 130 kW capacity is due to the formation of a more volumetric flame. This, in turn, leads to the formation of a more turbulent flow and increased recirculation ratio of the flue gases in the reacting zone. An increased burner capacity from 130 kW to 906 kW leads to an increase of the flame volume from 0.02 m³ to 2.6 m³, an increase of the turbulence intensity from 1.8% to 16%. With an increase of flame volume from case 1 to case 6, temperature drops, but total radiation heat flux increases.



1

Figure 1: Figure 1 :

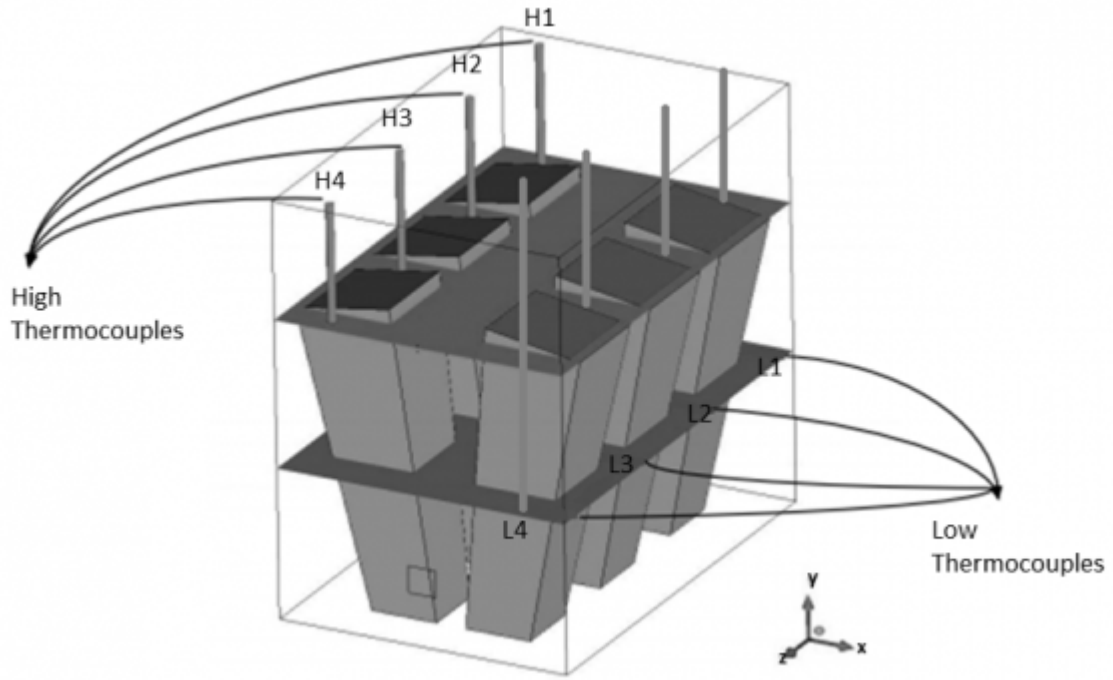


Figure 2:

316
317 1 2

¹Year 2017 G © 2017 Global Journals Inc. (US)
²© 2017 Global Journals Inc. (US)

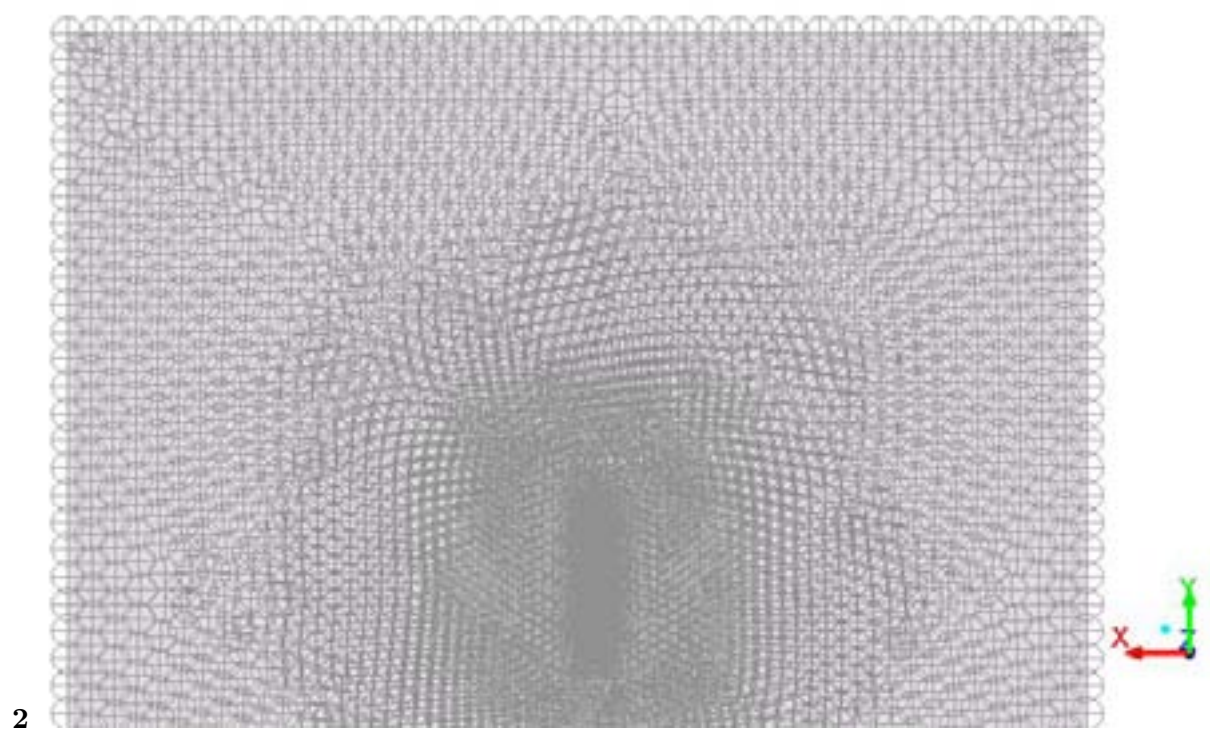
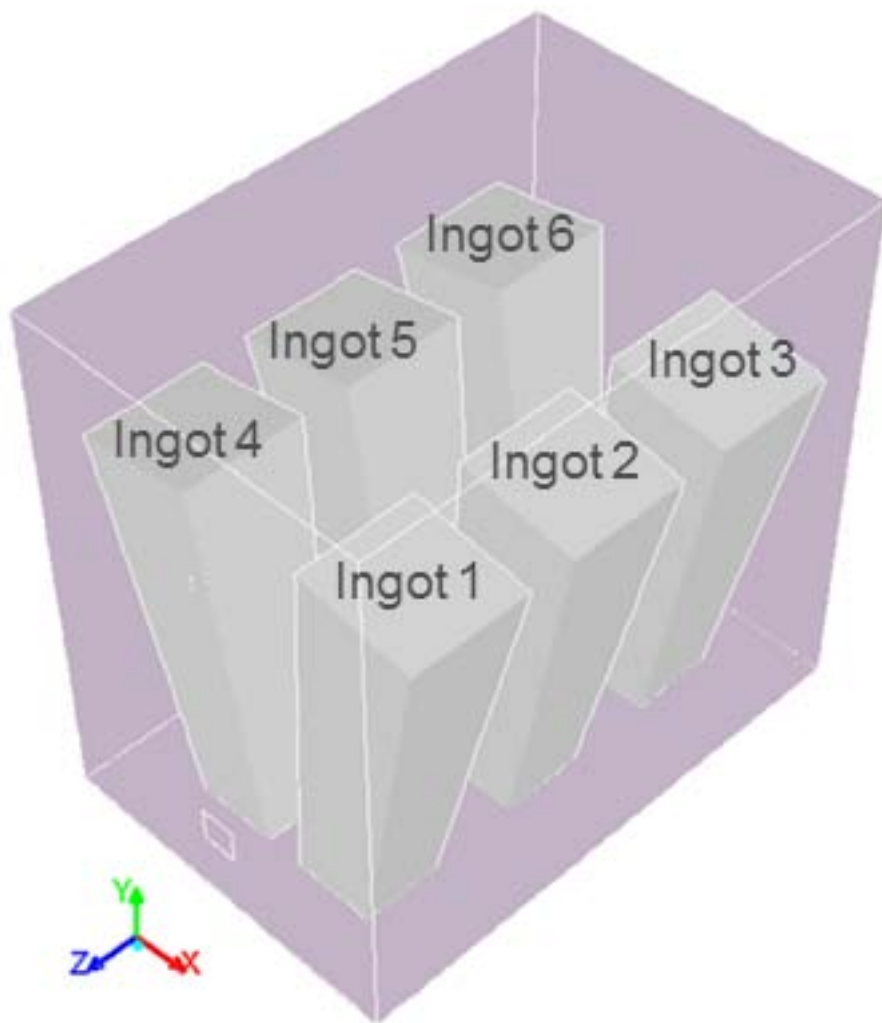
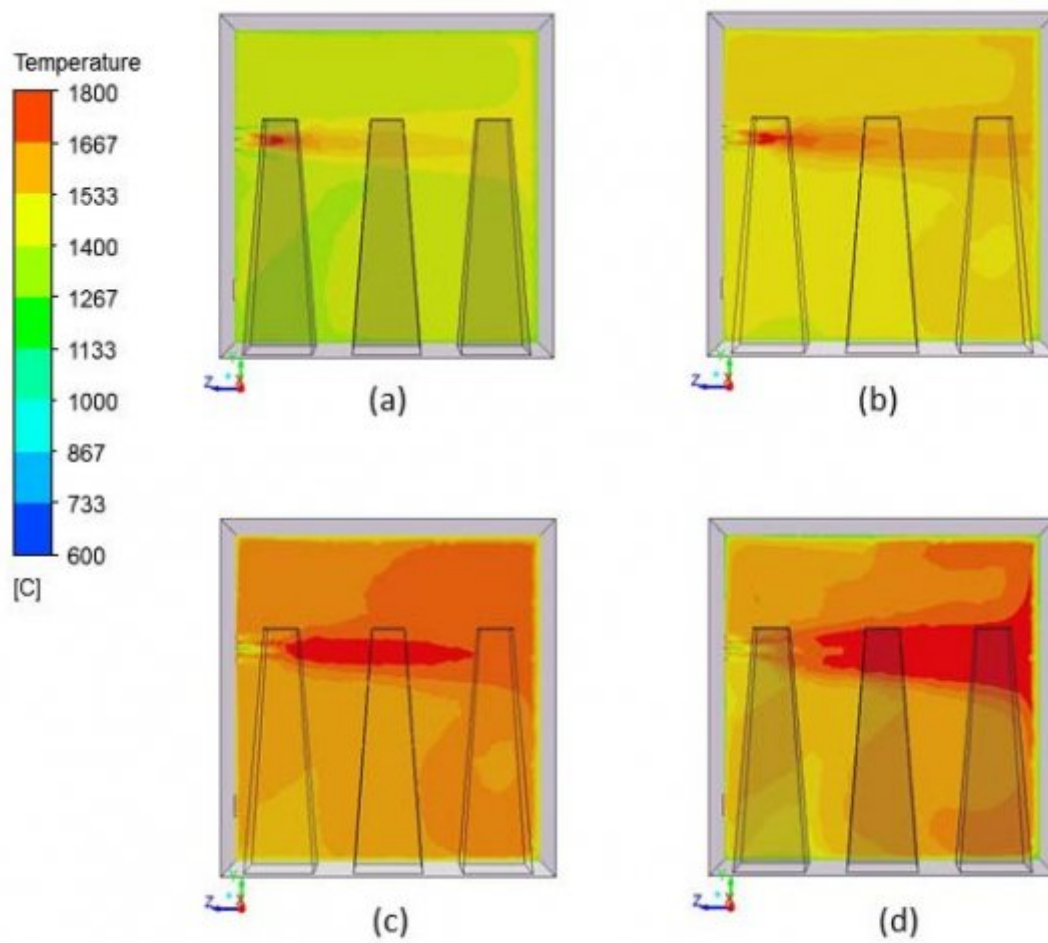


Figure 3: Figure 2 :



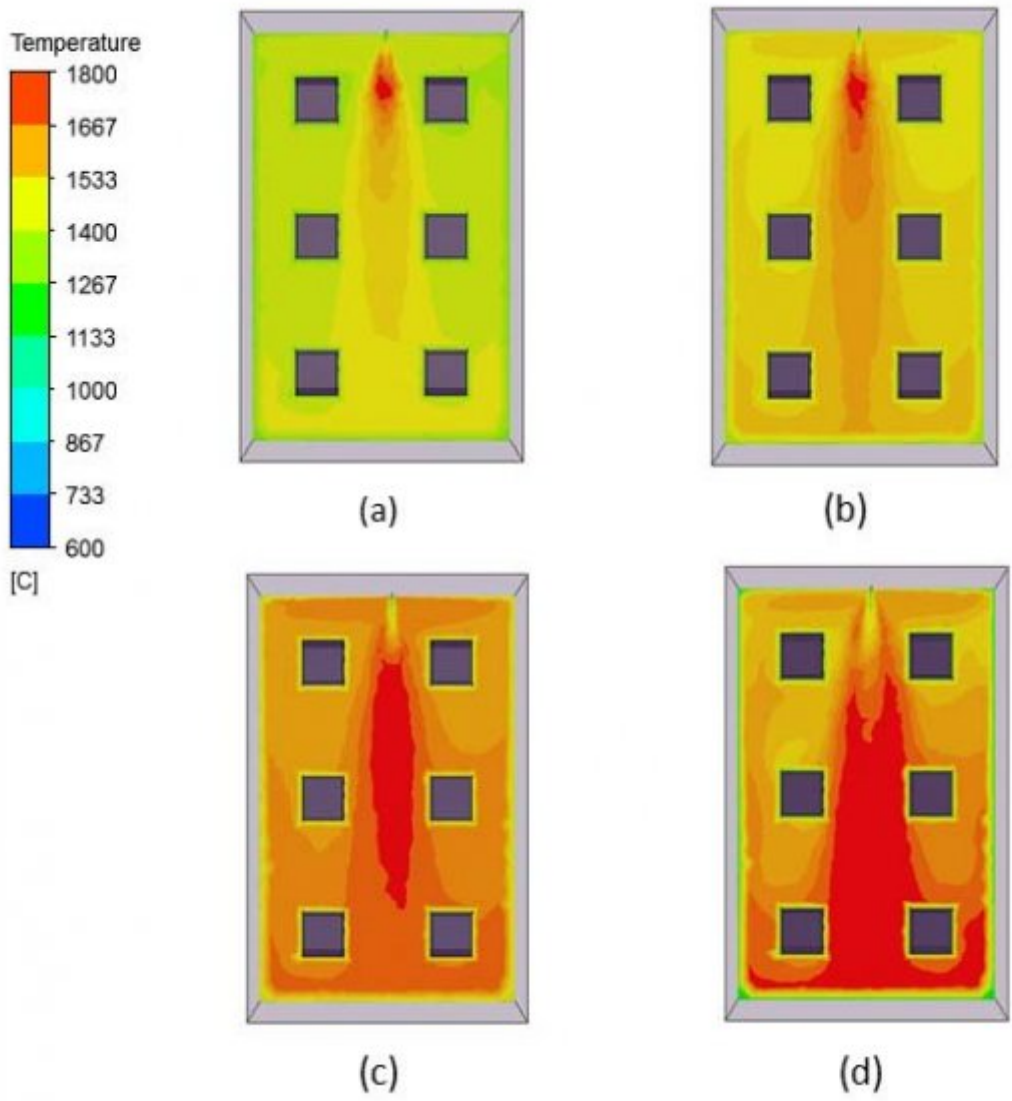
3

Figure 4: Figure 3 :



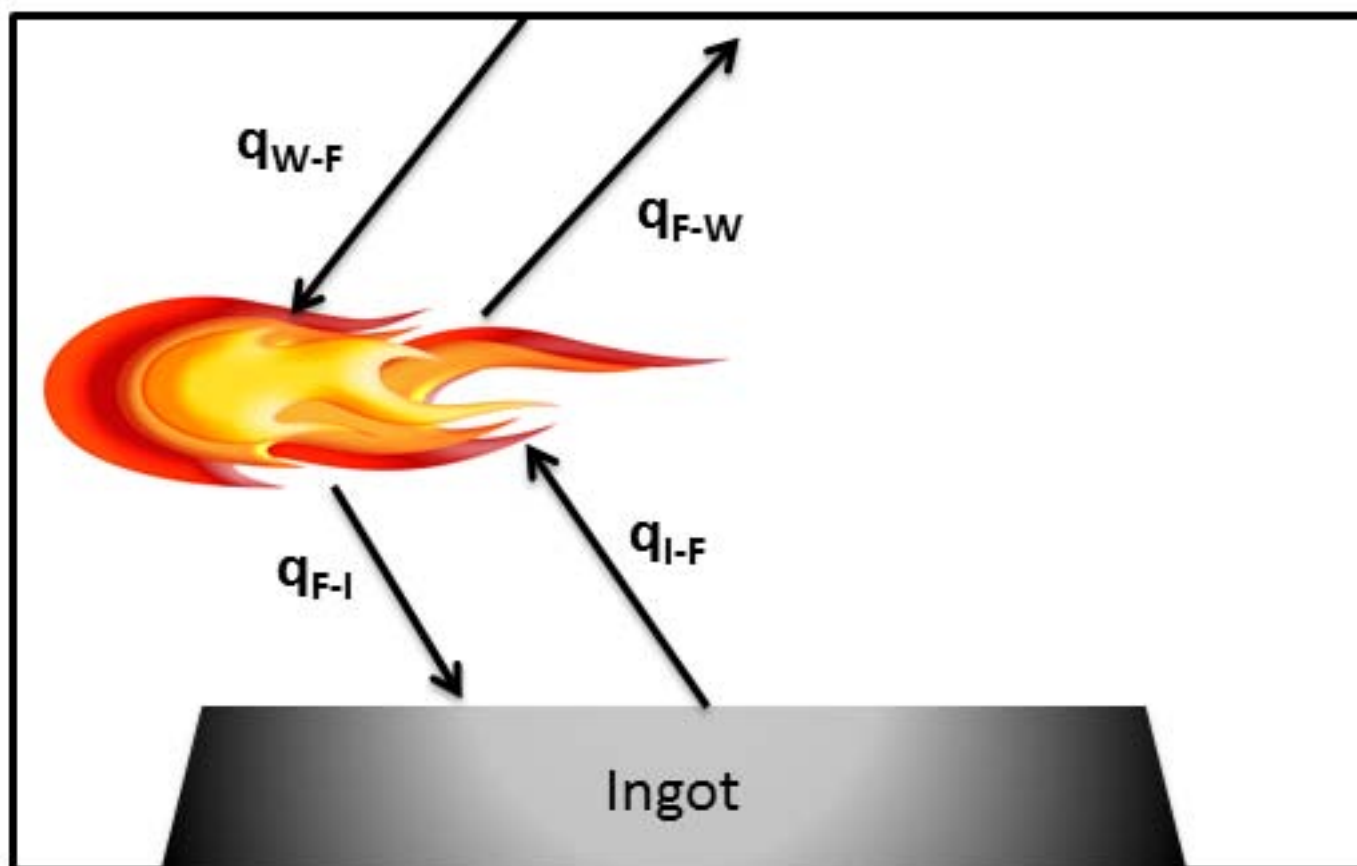
4

Figure 5: Figure 4 :



5

Figure 6: Figure 5 :A



6

Figure 7: Figure 6 :

2

| Thermocouple | Ref. | Low1 | High1 | Low2 | High2 | Low3 | High3 | Low4 | High4 |
|--------------|------|------|-------|------|-------|------|-------|------|-------|
| X (mm) | 910 | 1487 | 514 | 1487 | 514 | 1487 | 514 | 1487 | 514 |
| Y (mm) | 1105 | 1065 | 2065 | 1065 | 2065 | 1065 | 2065 | 1065 | 2065 |
| Z(mm) | 0 | 2631 | 2631 | 1810 | 1810 | 987 | 987 | 246 | 246 |

Figure 8: Table 2 :

1

| Parameter | Propane | Oxygen |
|-------------------------|---------|--------|
| Mass Flow (kg/s) | 0.013 | 0.06 |
| Inlet temperature (°C) | 22 | 25 |
| Hydraulic Diameter (mm) | 7 | 5 |
| Turbulent Intensity (%) | 5 | 6 |

Figure 9: Table 1 :

2

| Case Number | Inlet (Kg/s) | Fuel Rate | Inlet (Kg/s) | Oxygen Rate | ? | Burner Capacity(KW) |
|-------------|-----------------|--------------|-----------------|----------------|------|------------------------|
| CASE 1 | 0.002 | | 0.0074 | | 1.02 | 130 |
| CASE 2 | 0.005 | | 0.0185 | | 1.02 | 259 |
| CASE 3 | 0.008 | | 0.0296 | | 1.02 | 389 |
| CASE 4 | 0.011 | | 0.0407 | | 1.02 | 518 |

Figure 10: Table 2 :

3

| | | | | |
|-------------------------------|-----|-----|-----|-----|
| Heat loss (W/m ²) | 530 | 450 | 500 | 650 |
|-------------------------------|-----|-----|-----|-----|

Figure 11: Table 3 :

44. Flameless oxyfuel combustion: technology, La Revue de Métallurgie-CIT2006 1. Analysis of the experimental data collected during the 45. Oxygen-Enhanced Combustion, Second oxyflam-1 and oxyflam-2 experiments IFRF DocNo. Edition2013 ISBN 9781439862285 -CAT# K12887 F85/y/4 2. Oxy-fuel combustion technology for coal-fired power generation 4 Progress in Energy and Combustion Science

3. NO reduction in 0.03-0.2 MW oxy-fuel combustor using flue gas recirculation technology Proceedings of the Combustion Institute

4. Oxy-fuel (O₂/CO₂, O₂/RFG) the 30th international technical conference on coal utilization & fuel systems2005 5. NO Emission during Oxy-Fuel Combustion of Lignite Industrial and Engineering Chemistry research 6. Oxy-fuel combustion of solid fuels Progress in Energy and Combustion Science 7. Models for gaseous radiative heat transfer applied to oxy-fuel conditions in boilers 1-3 International Journal of Heat and Mass Transfer 8. Computational Fluid Dynamics Modeling of Oxy-Fuel Flames: The Role of Soot and Gas Radiation 5 energy and fuels 9. Experimental and numerical investigations on a swirl oxy-coal flame Applied Thermal Engineering 10. Numerical investigation of oxy-natural-gas combustion in a semi-industrial furnace: Validation of CFD sub-models Fuel 11. Oxygen-Enhanced Combustion CRC Press1998 12. Application of oxyfuel combustion in reheating at Ovako, Hofors works, Sweden -Background, solutions and results Linde AGA2006

Year 2017

31

()

Vol-ume XVII

Is-sue I

Ver-sion I

? The radiation from the flame to the ingots increases from 79.9 kW to 823.5 kW and the Q_{net}/Q_0 ratio increases from 0.36 to 0.85 with an increased Engineering 41. Evaluation of solution methods for radiative heat transfer in gaseous oxy-fuel combustion environments 14 Journal of Quantitative Spectroscopy and Radiative Transfer 42. Numerical Simulation of Combustion Characteristics

13. Flameless oxyfuel combustion: technology La Revue de Métallurgie-CIT 14. Flameless